

Numerical modeling of particle dynamics in a rotating disk chemical vapor deposition reactor

R.W. Davis, E.F. Moore and M.R. Zachariah

Chemical Science and Technology Laboratory, National Institute of Standards and Technology, Gaithersburg, Maryland 20899, USA

Received 22 December 1992; manuscript received in final form 10 May 1993

Particle contamination is considered to be one of the major problem areas in the processing of semiconductors via chemical vapor deposition (CVD). Thus it is very important to acquire an understanding of particle transport processes in CVD reactors. This paper addresses this issue by presenting the results of a numerical simulation of particle dynamics in a rotating disk CVD reactor. The background flowfield calculation employs the full axisymmetric Navier–Stokes equations, while individual particle trajectories are computed by accounting for inertial, thermophoretic and gravitational effects. The results of this simulation are analyzed to determine under what conditions particles greater than $1\ \mu\text{m}$ in diameter impact and thus contaminate the deposition substrate. It is shown that particle size and injection location as well as flow direction (with or against gravity) and disk characteristics (temperature and rotation rate) all play important roles here. The results for various parameter combinations are presented and discussed, as is the concept of a global type of particle contamination parameter.

Introduction

Particle contamination is considered to be one of the major limitations in the efficient processing of semiconductors during chemical vapor deposition (CVD). For micro-electronics fabrication of feature sizes less than $1\ \mu\text{m}$, as much as 75% of the yield loss can be attributed to particle contamination of the wafer. Since one of the major goals of the semiconductor industry is shrinkage of feature size, the particle contamination issue assumes great importance. There are two major sources of particle contamination: (1) cleanroom air, process gases and people in the cleanroom, and (2) new particle formation inside the CVD reactor through chemical and physical processes. Because of the extensive effort applied to controlling entry of particulates into the process, the first of these sources has largely been eliminated. At present, more than 80% of the total contaminant particles come from the chemical processing steps and the mechanical movement of equipment.

In order to develop methods for controlling contaminant motions inside CVD reactors, it is first necessary to understand the particle dynamics involved. Of particular concern is the question of under what conditions particles impact and thus contaminate the deposition substrate. The purpose of the present paper is to address this issue in the context of μm -size particles in the vertical rotating disk CVD reactor. The results of a numerical simulation of flow and particle dynamics in this type of reactor will be presented. These results indicate the major parameters influencing whether or not particles greater than $1\ \mu\text{m}$ in diameter impact the substrate, and thus provide possible mechanisms for contaminant control.

2. Vertical rotating disk CVD reactor

The configuration selected for this study is the vertical rotating disk CVD reactor (fig. 1). This configuration has been the subject of numerous

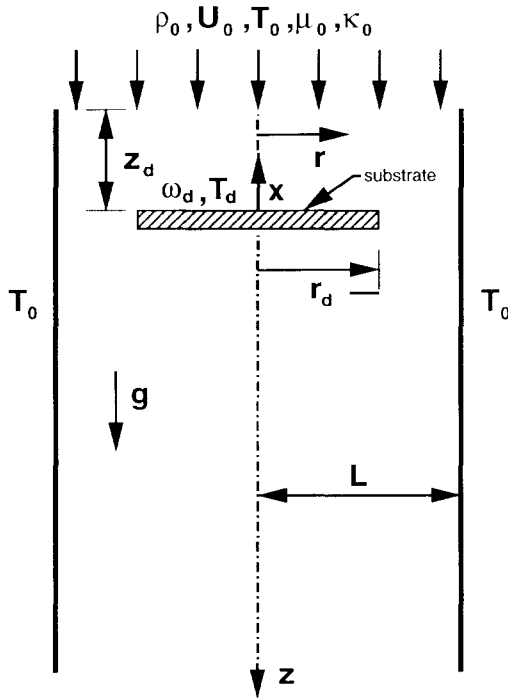


Fig. 1. Reactor configuration definition.

prior investigations (see Breiland and Evans [1]; Jensen, Einset and Fotiadis [2]) and has some important advantages associated with it. First, the simple geometry often results in very smooth axisymmetric flows which are highly amenable to both numerical modeling and laboratory experimentation. Note, however, that the reactor operating conditions must be carefully chosen so as to obtain these desirable types of flows. For example, a downward flow against a heated nonrotating disk will often result in unstable buoyant recirculation zones forming above the substrate [1,3], thus destroying the deposition process. Disk rotation will usually rectify this undesirable situation by creating a suction which entrains gas toward the disk and spins it out radially. This eliminates the recirculation zones and results in a highly uniform deposition layer. The second advantage of the vertical rotating disk reactor is that a reduced set of flow variables (von Karman transformation [4]) can often be employed in solution procedures over a large central portion of the disk. This reduced set of variables, dependent

only on an axial coordinate, is obtained by assuming at most a linear dependence on radius over an infinite disk [1]. The resulting system of flow equations in only one dimension can then be solved both rapidly and efficiently. In particular, this allows for the detailed computation of chemical kinetic effects [5], a procedure which is extremely arduous in multidimensions.

The insertion and tracking of individual particles through the vertical rotating disk reactor is fairly straightforward because of the smoothness of the gaseous flowfield under typical operating conditions. Particles either impact the disk or are carried around it and out of the reactor. The present investigation concentrates on determining the critical parameters (e.g., spin rate, disk temperature, particle size) which influence how close an individual particle gets to the disk. The axisymmetric gas flowfield computation is carried out utilizing the full multidimensional Navier–Stokes equations, while particle trajectories are calculated by applying drag, thermophoretic and gravitational forces to individual particles. The next section details the computational technique.

3. Flowfield and particle transport modeling

The axisymmetric nondimensional continuity, momentum, energy and state equations employed here for the flowfield computations are:

$$\frac{\partial \rho}{\partial t} + \nabla \cdot (\rho \mathbf{q}) = 0, \quad (1)$$

$$\begin{aligned} \rho \frac{\partial \mathbf{q}}{\partial t} + \rho (\mathbf{q} \cdot \nabla) \mathbf{q} \\ = -\nabla \bar{p} + \rho \text{ Ri } \hat{e}_z + \frac{1}{\text{Re}} \left[-\nabla \times (\nabla \times \mu \mathbf{q}) \right. \\ \left. + \frac{4}{3} \nabla (\mu \nabla \cdot \mathbf{q}) + \nabla (\mathbf{q} \cdot \nabla \mu) - \mathbf{q} \nabla^2 \mu \right. \\ \left. + \nabla \mu \times (\nabla \times \mathbf{q}) - (\nabla \cdot \mathbf{q}) \nabla \mu \right], \end{aligned} \quad (2)$$

$$\rho \frac{\partial T}{\partial t} + \rho (\mathbf{q} \cdot \nabla) T = \frac{1}{\text{Re Pr}} \nabla \cdot (\kappa \nabla T), \quad (3)$$

$$\rho = \rho_0 / RT. \quad (4)$$

Here ρ is density, μ is viscosity, κ is thermal conductivity, T is temperature, $\mathbf{q} = (v, w, u)$, where v , w , and u are radial, azimuthal and axial velocity components, respectively, in an axisymmetric reference frame (r, z) (fig. 1), R is gas constant, and \hat{e}_z is the unit normal in the axial direction. The pressure consists of a constant background pressure, p_0 , plus a perturbation pressure, $\tilde{p}(r, z, t)$, where $p_0 \gg \tilde{p}$ (i.e., the low Mach number approximation [6]). All quantities in eqs. (1)–(4) have been nondimensionalized with respect to the reactor radius, L , and conditions in the entering flow (fig. 1). Thus, $\text{Re} = \text{Reynolds number} = \rho_0 U_0 L / \mu_0$, $\text{Ri} = \text{Richardson number} = gL / U_0^2$, and $\text{Pr} = \text{Prandtl number} = \mu_0 C_p / \kappa_0$, where the specific heat C_p is assumed constant. Note that time derivatives have been retained in eqs. (1)–(3) in spite of the fact that the flowfields under consideration here are steady. This is to enable future use of this model to study unsteady effects in these types of reactors. For the present study, the finite difference solution procedure progresses until the time derivatives become negligible. This procedure utilizes a variably-spaced staggered mesh in which pressures are defined at cell centers and normal velocities at cell faces. Quadratic upwind differencing is used for convection, and an explicit Leith-type of temporal differencing is employed [7]. At each time step, a Poisson equation for perturbation pressure is solved by a direct method [7]. This is therefore a fully elliptic algorithm capable of simulating any recirculation zones which may be present. As can be seen in fig. 2, a total of 86 variably-spaced grid cells are employed in the axial direction over a length of $16L$, while there are 54 cells radially. The upstream surface of the rotating disk is at about $z_d = 2.6L$. The disk is about $0.4L$ thick and has a radius, r_d , of $0.67L$. These conditions, along with the particular boundary conditions yet to be discussed, were chosen so as to simulate experiments performed by Breiland and Evans [1], for which $L = 4.75$ cm.

The boundary conditions for the flowfield computations assume a uniform entrance velocity profile, U_0 , and known flow properties. Both the entrance flow and the reactor walls are maintained at $T_0 = 293$ K, while the disk surface is

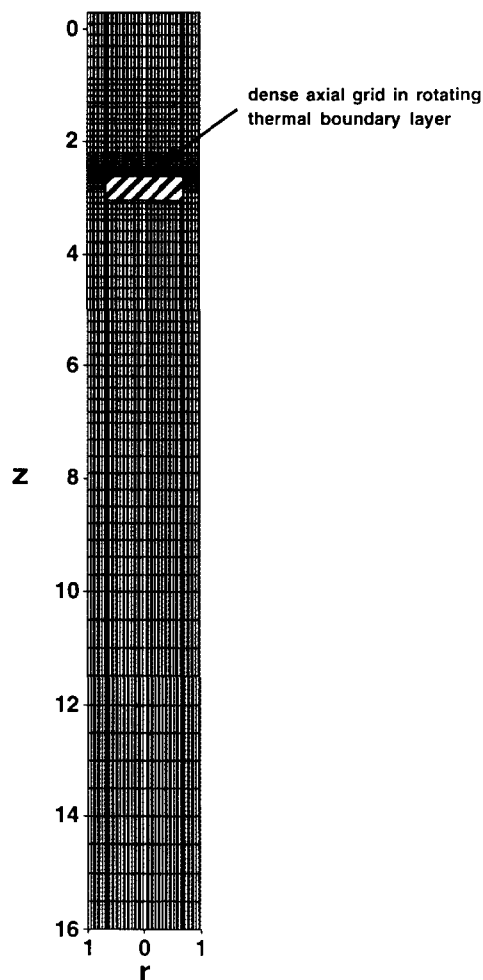


Fig. 2. 86 (axial) \times 54 (radial) computational grid; alternate radial grid lines removed.

maintained at temperature T_d . No-slip boundary conditions apply along the reactor walls and the disk, which is spinning at angular velocity ω_d . The background pressure, p_0 , is specified. The outflow boundary conditions at $z = 16L$ are obtained by local applications of mass conservation and streamwise extrapolations. These permit the flow to exit the mesh with as little disturbance as possible. Thus, there are no a priori assumptions regarding spatial gradients at this boundary. Finally, axisymmetry is enforced along the reactor centerline. Also, the viscosity and thermal conductivity are assumed to vary with temperature

as: $\mu \propto T^{0.6756}$ and $\kappa \propto T^\alpha$, where α is species dependent [8].

Following the computation of steady reactor flow and temperature fields, individual particles are injected near the entrance ($L \leq z \leq 2L$) with the local flow velocity and their trajectories computed. The particle dynamics is as described by Fotiadis and Jensen [9]. Each particle is considered as an isolated small sphere whose Brownian diffusivity is negligible compared with the surrounding gas diffusivity. The drag force is calculated assuming that both the particle Reynolds number and the Knudsen number ($\text{Kn} = \lambda/r_p$, where $\lambda =$ gas molecule mean free path and $r_p =$ particle radius) are less than unity. The thermophoretic force is computed by means of an interpolating formula derived by Talbot et al. [10] to span a range of small Knudsen numbers. Thus

$$m \, d\mathbf{q}_p/dt = \mathbf{F}_d + \mathbf{F}_T + \mathbf{F}_g, \quad (5)$$

where

$\mathbf{F}_d =$ drag force

$$= \frac{-6\pi\mu(\mathbf{q}_p - \mathbf{q})r_p}{1 + \text{Kn}(1.2 + 0.41 e^{-0.88/\text{Kn}})},$$

$\mathbf{F}_T =$ thermophoretic force

$$= \frac{-\pi\mu^2 r_p \nabla T}{\rho T} \times \frac{13.764(\kappa/\kappa_p + 2.2 \text{Kn})}{(1 + 3.438 \text{Kn})(1 + 2\kappa/\kappa_p + 4.4 \text{Kn})},$$

$\mathbf{F}_g =$ gravitational force $= mg$.

Here m is the mass of a spherical particle of radius r_p and thermal conductivity κ_p moving with velocity \mathbf{q}_p . A particle's position along its trajectory is updated by simply integrating eq. (5) twice assuming a constant flow velocity over the very small integration time interval. Particles that impact the disk are terminated (i.e., inelastic collision), while the remainder of the particles are tracked until they are well downstream of the disk.

The flowfield computations for this study have been carried out on the NIST CRAY Y-MP, with

typically 2 h of CPU time required per case. The particle trajectory computations and analysis have been performed on Silicon Graphics workstations, where less than 1 min is typically required to calculate and display trajectories for 10 particles.

4. Results and discussion

The baseline flowfield selected for this study utilizes a parameter set taken from Breiland and Evans [1]. The purpose of this is to enable comparison with their experimental temperature profiles inside the boundary layer region above the substrate. The geometry of their reactor is as described previously. The carrier gas is hydrogen ($\alpha = 0.768$) entering at temperature $T_0 = 293$ K with velocity $U_0 = 9.4$ cm/s. The background pressure is $p_0 = 0.829$ atm. The heated disk ($T_d = 908$ K) is spinning at $\omega_d = 1000$ rpm. Thus, the relevant nondimensional parameters are $\text{Re} = 35$,

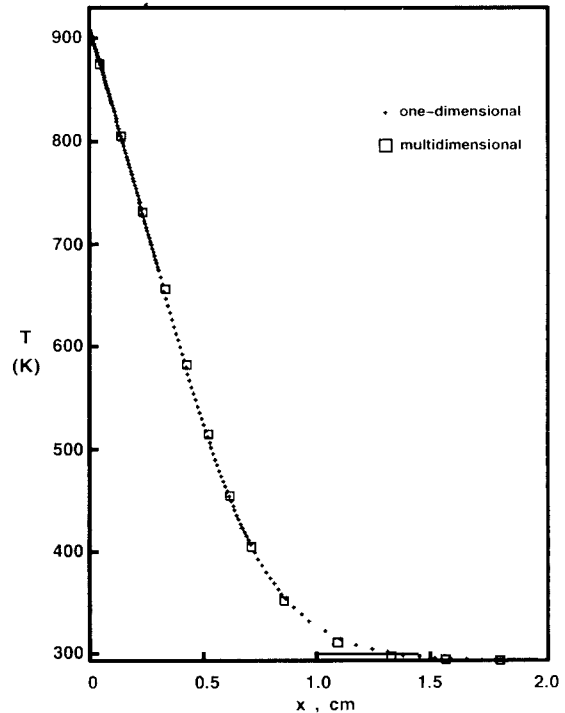


Fig. 3. Boundary layer temperature comparison.

$Ri = 52.7$ and $Pr = 0.71$. As shown in Breiland and Evans [1], the experimental boundary layer temperature profiles over the inner 2/3 of the disk are virtually coincident with profiles computed via the one-dimensional von Karman variables. Thus, employing the one-dimensional SPIN code developed at Sandia National Laboratories [11], a comparison of calculated temperatures has been made between the von Karman solution for this case and the results along the reactor centerline of the full axisymmetric computations utilizing eqs. (1)–(4). This comparison, shown in fig. 3, indicates that the full axisymmetric flowfield solver is performing well and consideration of the particle dynamics can thus commence.

The simplest situation involving particle dynamics in this reactor is the baseline case described above but with no disk rotation. Thus a

particle-laden flow would be directed down against a heated stationary disk. Unfortunately, as noted previously, this type of flow often results in unstable, buoyant recirculation zones above the substrate, a condition which in fact occurs here. Thus no acceptable numerical solution was found for this case. The most obvious remedy for this problem is to invert the reactor, i.e., direct flow up (instead of down) against the substrate. Therefore, this will be the first case to be considered in the discussion on particle dynamics in this type of reactor.

Fig. 4 shows five particle trajectories in the region of the flow near the substrate. The particles are given the properties of silicon with a density of 2.33 g/cm^3 and a thermal conductivity of $0.312 \text{ W/cm} \cdot \text{K}$. These particles have a diameter of $5 \mu\text{m}$ and are injected at different radial

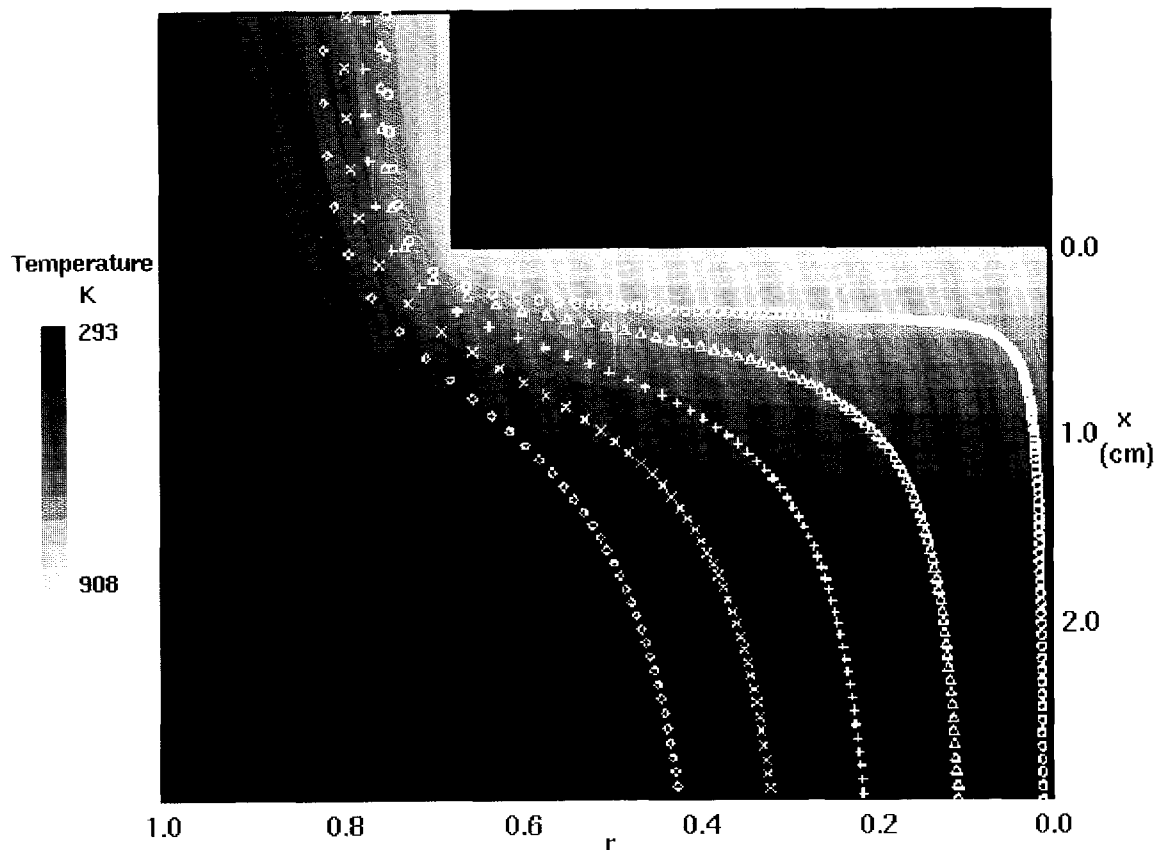


Fig. 4. Trajectories of $5 \mu\text{m}$ diameter particles through inverted reactor with no disk rotation.

locations. Each trajectory is indicated by its own symbol against a contour map of temperature surrounding the 908 K disk. Note that none of the particles impacts the substrate. The axial forces acting on one of these particles along part of its trajectory are shown in fig. 5. Each force is normalized with respect to the magnitude of the gravitational force on the particle ($=|-1|$), where a negative sign indicates a force acting in the x -direction (repellent). Note that since the particle is inserted in the flow with the local gas velocity at $x = 2.04$ cm, the drag force initially rises rapidly as the particle decelerates under the influence of gravity. Both the drag and thermophoretic forces acting on the particle increase in magnitude (although in opposite directions) as the particle penetrates the thermal boundary layer

adjacent to the substrate. Note, though, that the total force (including gravitational) remains very slightly repellent prior to the turn in the trajectory at about $x = 0.5$ cm. The effect of varying particle size at the five injection locations of fig. 4 is shown in fig. 6. Here the closest approach to the substrate (x_{\min} , cm) over each trajectory is plotted against particle diameter, with $x_{\min} = 0$ implying impact. Note from fig. 4 that x_{\min} often occurs near the outer edge of the disk. As can be seen from fig. 6, no impacts are indicated. In fact, none of the particles gets closer to the substrate than about 1.7 mm, with x_{\min} increasing with injection radius. As the particle size increases, the repellent gravitational force becomes increasingly important, which leads to progressively less penetration of the boundary layer.

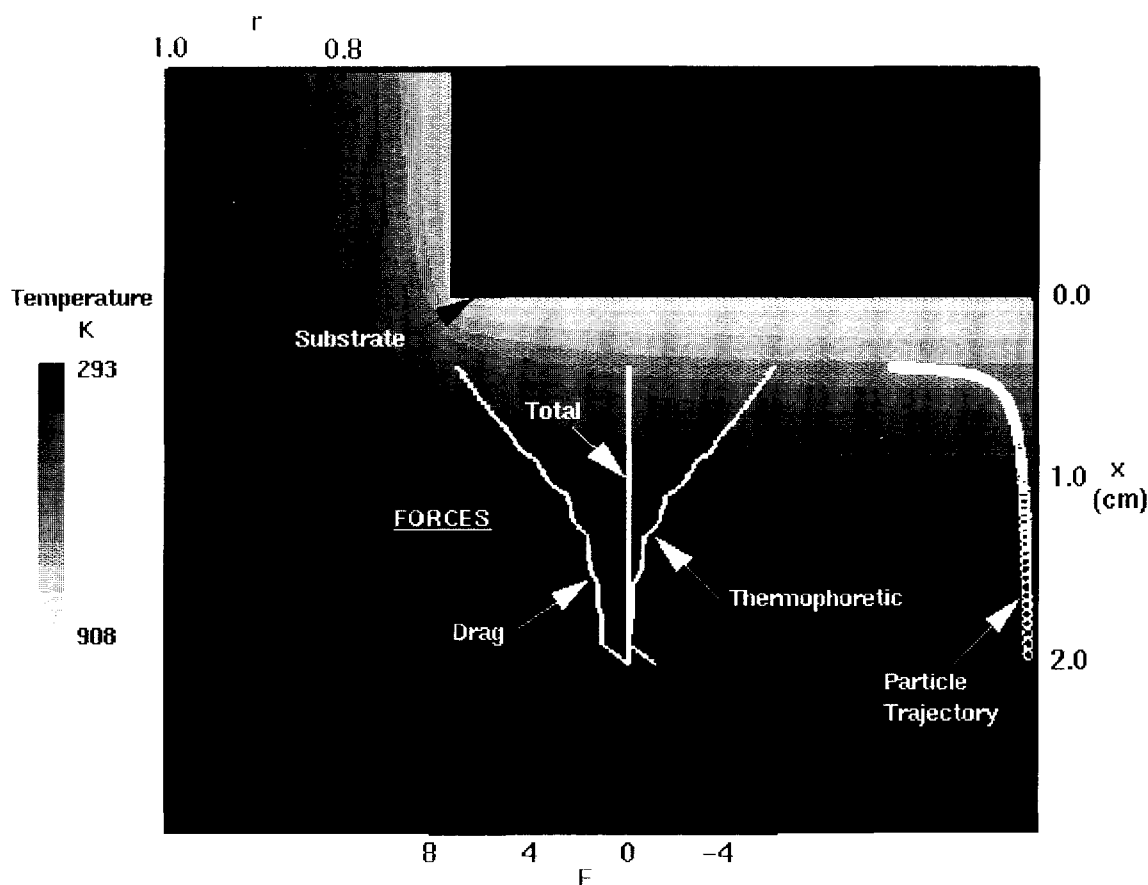


Fig. 5. Axial forces acting on a $5 \mu\text{m}$ diameter particle in inverted reactor with no disk rotation.

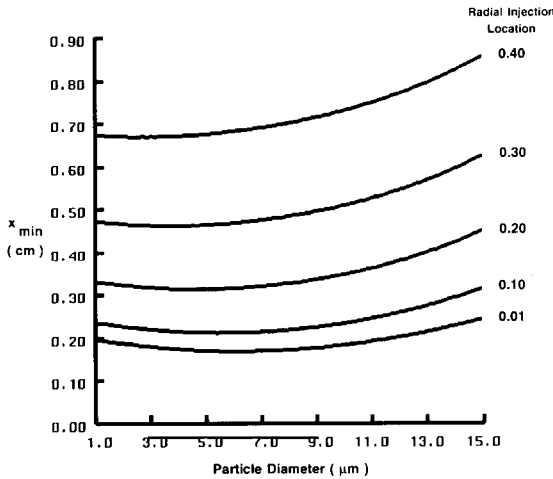


Fig. 6. Closest approach to substrate for particles in inverted reactor with no disk rotation.

The case just discussed had a substrate temperature of 908 K, which is rather low for silicon epitaxy [2]. Fig. 7 shows the effect on boundary layer penetration of increasing this temperature to a more realistic value of 1250 K. As is evident at the two injection locations shown, the increased temperature results in significantly larger values of x_{min} for the smaller particles most affected by thermophoresis. As particle size in-

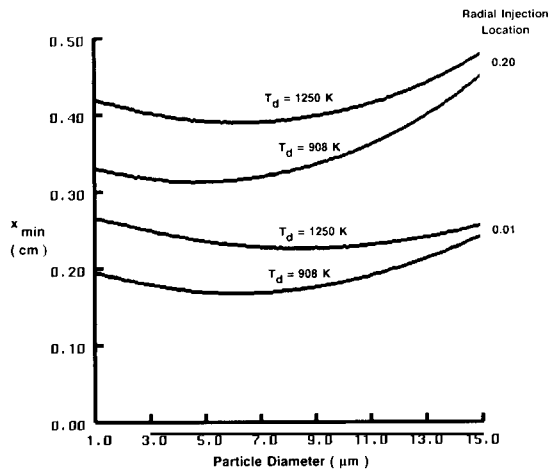


Fig. 7. Effect of disk temperature on closest approach to substrate for particles in inverted reactor with no disk rotation.

creases, gravitational effects become dominant and temperature differences matter less.

The final comparison involving the inverted reactor is intended to demonstrate the effects of disk rotation. From fig. 8 it can be seen that values of x_{min} with a rotating disk (1000 rpm) are approximately half those without rotation for the two radial injection locations chosen. This is due to the rotation-induced suction which pulls the particles toward the substrate. Note that this suction also diminishes the dominant role of gravity as particle size increases.

The baseline rotating case of Breiland and Evans [1] that was previously discussed will now be considered with the addition of particle dynamics. Fig. 9 is analogous to fig. 4 in that it shows the trajectories in the rz plane of $5 \mu\text{m}$ diameter particles through the flow surrounding the disk. In the case of fig. 9, however, the disk is rotating at 1000 rpm and gravity acts in the $-x$ -direction. Note that the spin-induced swirl changes the three-dimensional nature of the trajectories, causing the particles to spiral in toward and then around the disk, as shown in fig. 10. The trajectories seen here resemble those observed experimentally by means of smoke wire visualizations [1]. The parameter changes from the nonrotating inverted case result in a narrower boundary layer and deeper particle penetration as suction and gravity now act to decrease x_{min} . This

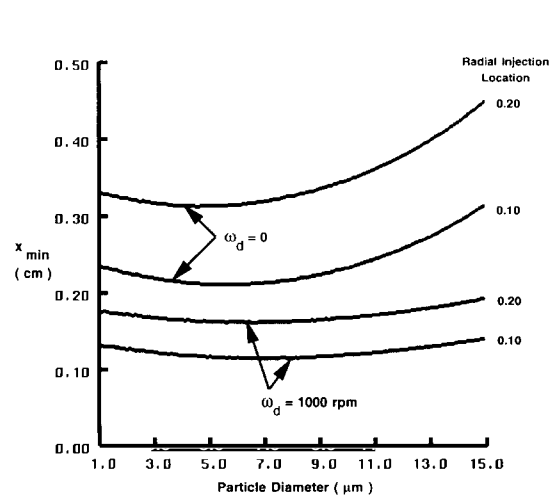


Fig. 8. Effect of disk rotation on closest approach to substrate for particles in inverted reactor with $T_d = 908 \text{ K}$.

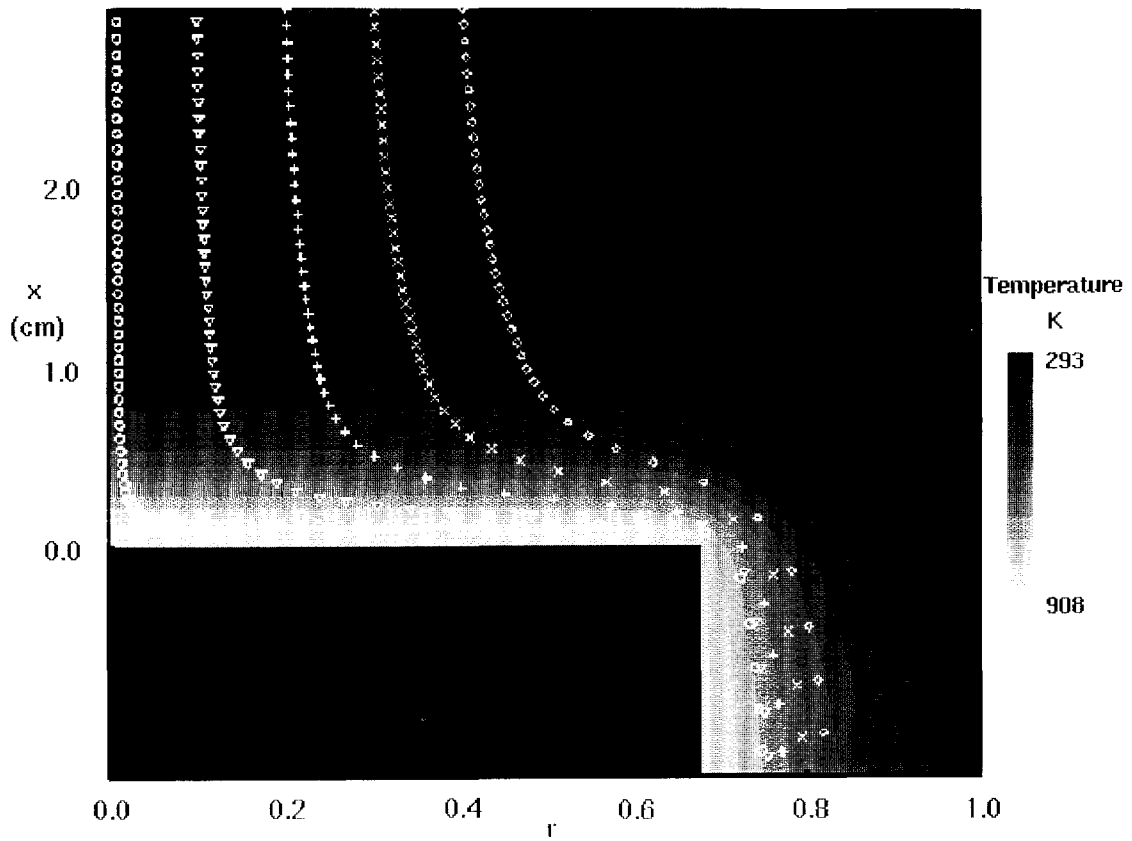


Fig. 9. Trajectories of 5 μm diameter particles through baseline rotating disk reactor.

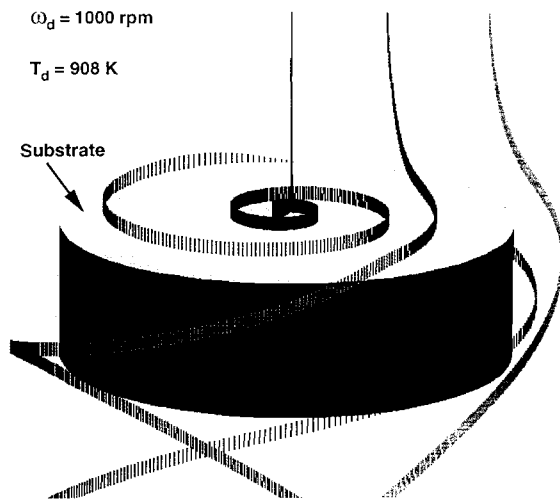


Fig. 10. Spiral trajectories of three 5 μm diameter particles through baseline rotating disk reactor.

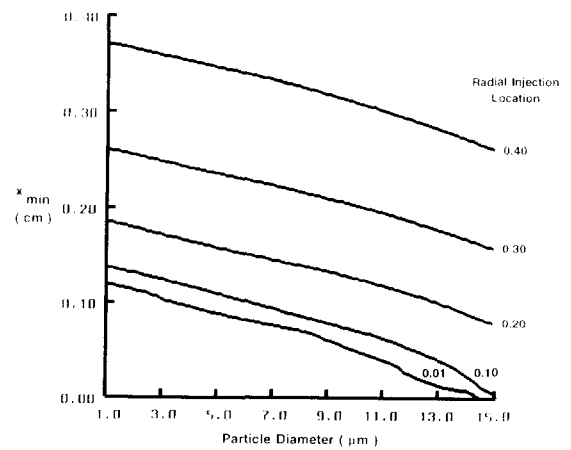


Fig. 11. Closest approach to substrate for particles in baseline rotating disk reactor.

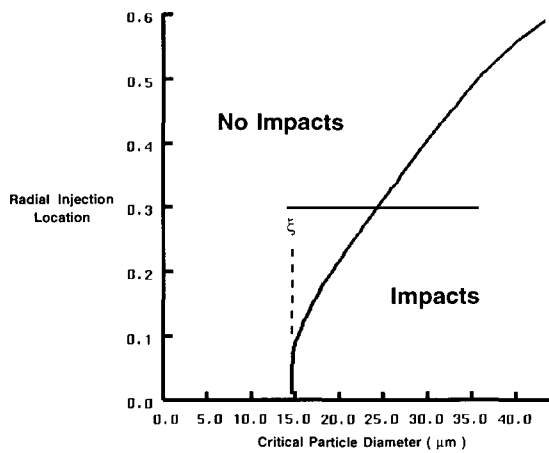


Fig. 12. Critical particle diameters for baseline rotating disk reactor.

can be seen by comparing fig. 11 with fig. 6. Fig. 11, which presents x_{\min} as a function of particle size and injection radius for the baseline rotating case, clearly shows much smaller values of x_{\min} than seen in fig. 6. In fact, particle impact ($x_{\min} \rightarrow 0$) occurs for the two inner radial injection locations for particle diameters of approximately $15 \mu\text{m}$. Thus, unlike the inverted nonrotating case, impact is a possibility here.

In order to quantify the impact possibilities for this reactor configuration, fig. 12 presents critical particle diameter as a function of radial injection location. Particles larger than the critical value for any given injection location will impact the substrate. Thus, all particles with diameter greater than about $15 \mu\text{m}$ that are injected near the reactor centerline for this case will impact. As radial injection location increases, so too does the critical particle diameter. Thus, the global critical particle diameter, ξ , for this case is approximately $15 \mu\text{m}$; i.e., no particles smaller than this (and $> 1 \mu\text{m}$ diameter) will impact the substrate regardless of injection radius. Increasing the substrate temperature from 908 to 1250 K results in an increase in ξ to $20 \mu\text{m}$. This can be noted from table 1, where the effects on ξ of changes in ω_d and T_d are listed. For the unheated substrate ($T_d = 293 \text{ K}$), there is no repellent thermophoretic force. Consequently all particles injected in the central region of the reactor will

Table 1

Global critical particle diameter for various cases

ω_d (rpm)	T_d (K)	ξ (μm)
1000	1250	20
1000	908	15
1000	615	10
1000	293	0
500	908	13

impact. Lowering the spin rate from 1000 to 500 rpm results in a slight decrease in ξ . In fact, the critical particle diameters for the latter case are slightly smaller than in the baseline case for small radial injection locations (≤ 0.2) and slightly greater for large radial injection locations. If the background reactor pressure is reduced by half ($p_0 = 0.415 \text{ atm}$) for the baseline case ($\omega_d = 1000 \text{ rpm}$, $T_d = 908 \text{ K}$), the value of ξ increases to $22 \mu\text{m}$. This is because reducing the pressure correspondingly reduces the gas density which leads to a greater thermophoretic force on the larger particles. Thus, raising substrate temperature and lowering background pressure are effective and practical means of reducing particle impacts in this type of reactor. Finally, another extremely effective, though impractical, method for reducing impacts in the baseline case is to operate the reactor in a zero-g environment, for which $\xi = 54 \mu\text{m}$. As noted previously, reactor inversion for

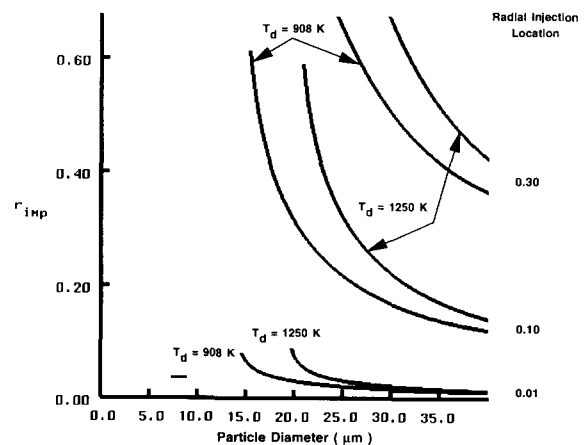


Fig. 13. Effect of disk temperature on radial impact location for particles in baseline rotating disk reactor.

this case is even more effective, i.e., no impacts (see fig. 8), and is far more practical.

The radial locations at which particles impact the substrate (r_{imp}) are presented in fig. 13 for both the baseline case and the increased disk temperature case ($T_d = 1250$ K). For a radial injection location of 0.3, particles near the critical particle diameter of approximately $25 \mu\text{m}$ impact near the edge of the disk (recall $r_d = 0.67$). As particle size increases for all three radial injection locations shown, r_{imp} decreases as inertial effects become increasingly dominant. Raising the disk temperature from 908 to 1250 K increases r_{imp} as the larger thermophoretic force delays impact.

5. Conclusions

A numerical simulation of particle dynamics in a rotating disk CVD reactor has been carried out utilizing a full Navier–Stokes flowfield solver and individual particle trajectory computations. The primary focus here has been on identifying the factors which influence particle impaction, and thus contamination, of the deposition substrate. A very useful parameter, the global critical particle diameter ξ , has been identified which indicates the minimum impaction size over all particle locations in the reactor. Note that ξ does not account for submicron particles which can undergo significant diffusion and thus are not amendable to the particle trajectory type of analysis employed here. It has been seen that ξ increases with disk temperature (due to increased thermophoresis) and decreases with reactor pressure, and is not strongly dependent on rotation rate. Inverting the reactor (flow up instead of

down) negates adverse buoyancy effects near a nonrotating disk and eliminates particle impacts altogether in both the rotating and nonrotating cases.

The concept of an overall reactor particle contamination parameter such as ξ could prove useful in design considerations. Operating conditions with smaller values of ξ can be considered as more contamination prone than those with larger values. Thus, variations in the value of ξ due to changes in reactor design or operating conditions could be one element employed to assess the desirability of these changes. Extension of this concept to other types of reactors (e.g., the horizontal reactor [9]) certainly appears feasible.

References

- [1] W.G. Breiland and G.H. Evans, *J. Electrochem. Soc.* 138 (1991) 1806.
- [2] K.F. Jensen, E.O. Einset and D.I. Fotiadis, *Ann. Rev. Fluid Mech.* 23 (1991) 197.
- [3] C.R. Biber, C.A. Wang and S. Motakef, *J. Crystal Growth* 123 (1992) 545.
- [4] H.P. Greenspan, *The Theory of Rotating Fluids* (Cambridge University Press, Cambridge, 1969) ch. 3, p. 133.
- [5] M.E. Coltrin, R.J. Kee and G.H. Evans, *J. Electrochem. Soc.* 136 (1989) 819.
- [6] R.G. Rehm and H.R. Baum, *J. Res. Natl. Bur. Std. (US)* 83 (1978) 297.
- [7] R.W. Davis and E.F. Moore, *Phys. Fluids* 28 (1985) 1626.
- [8] R.E. Mitchell, Report No. SAND 79-8236, Sandia National Laboratories, Livermore, CA (1980).
- [9] D.I. Fotiadis and K.F. Jensen, *J. Crystal Growth* 102 (1990) 743.
- [10] L. Talbot, R.K. Chen, R.W. Schefer and D.R. Willis, *J. Fluid Mech.* 101 (1980) 737.
- [11] M.E. Coltrin, R.J. Kee, G.H. Evans, E. Meeks, F.M. Rupley and J.F. Grcar, Report No. SAND 91-8003, Sandia National Laboratories, Albuquerque, NM (1991).